IEEE Access
Multidisciplinary | Rapid Review | Open Access Journal

Received October 3, 2018, accepted October 20, 2018, date of publication October 24, 2018, date of current version November 30, 2018.

Digital Object Identifier 10.1109/ACCESS.2018.2877782

An Electronically Mode Reconfigurable Orbital Angular Momentum Array Antenna

YAN-YANG WANG, YONG-XING DU, LING QIN, AND BAO-SHAN LI
School of Information Engineering, Inner Mongolia University of Science and Technology, Baotou 014010, China

Corresponding author: Yong-Xing Du (dyxql@imust.edu.cn)

This work was supported in part by the National Nature Science Foundation of China under Grant 61661044 and Grant 61501266 and in part by the Technology Innovation Research Project—Outstanding Youth Science Fund Project of Inner Mongolia University of Science and Technology—under Grant 2017YQL10

ABSTRACT In this paper, an array antenna for generating multi-mode orbital angular momentum (OAM) vortex waves and having electrically controlled mode reconfigurable function is proposed. The proposed antenna is based on a reconfigurable feed network (RFN) consisting of multiple PIN diodes as reconfigurable switches, a direct current (dc) control board and a 2×4 radial uniform circular array. By controlling the coding sequence of the corresponding PIN diode dc bias voltage on the RFN using a programmable microcontroller, the OAM modes generated by the proposed antenna can be dynamically reconfigured between $l = 0$, ± 1, and ± 2. Moreover, the OAM beams can be generated in a wide frequency band of 5.5–6.1 GHz and 5.65–6.1GHz for $l = \pm 1, \pm 2$ modes and $l = 0$ mode, respectively. The prototype of the proposed antenna is simulated and fabricated to validate the proposed design. Both far-field and near-field experiments were performed to verify the feasibility of the proposed design. The results of the numerical simulation and measurement have good agreement with each other.

INDEX TERMS Reconfigurable, orbital angular momentum (OAM), PIN didoes, array antenna.

I. INTRODUCTION

Nowadays, with the rapid development of wireless communication technologies for information exchange, the number of mobile terminals has increased dramatically, and the mobile Internet has shown an explosive development trend. In order to meet the growing demand for mobile data services, there is an urgent need for a new generation of wireless communication technologies with higher speed, greater bandwidth, and higher efficiency. Electromagnetic vortex beam orbital angular momentum (OAM) becomes the fifth new dimension that is expected to improve spectrum efficiency beyond the four dimensions of amplitude, phase, frequency, and polarization that electromagnetic waves have been utilized. It is common knowledge that electromagnetic waves can carry the linear momentum as well as angular momentum, which is divided into spin angular momentum (SAM) and OAM [1]. The OAM describes the spatial coordinate dimension of the spiral beam transverse rotation mode which is perpendicular to the Poynting vector direction, and the SAM corresponds to the polarization of the electromagnetic wave. The transmission of information by modulating the OAM of electromagnetic fields is first proposed in the field of optics. Since then, the use of OAM for spatial optical communication has become a hot topic in the world [2]. Recently, the OAM has received great attention in the field of radio frequency wireless communication, since, it is possible to modulate the multiplexed signals in different OAM modes by using the mutual orthogonal characteristics between the OAM modes, and distinguish different channels according to the modes, then multiple signals can be transmitted under the same carrier frequency to achieve the purpose of improving spectrum utilization. The vortex electromagnetic wave is characterized by a helical phase factor $\exp(-il\phi)$ in the expression of the field, where l represents the quantum topological charge that can take any integer value, also called the mode number of OAM, and ϕ represents the azimuth angle [3].

So far, there are mainly three methods that have been proposed for generation of OAM radio beams in the microwave and RF bands. The first type of OAM antenna structure is spiral phase plate (SPP) [4], [5], the second type of OAM antenna structure is spiral phase reflector [6], the third type of OAM antenna structure is uniform circular array [7]–[9]. Furthermore, by using four-dimensional antenna arrays, multiple OAM modes can be generated by a single antenna [10].

Various simple and compact OAM antennas have been reported, such as dielectric resonator [11]–[13], grapheme metamaterial reflectarray [14]. However, most of the antennas mentioned above have problems in that the number of OAM modes is small, the narrowband, and the mode are not reconfigurable.

Modern communication systems are characterized by diversified functions and diverse working environments. The characteristics of traditional antennas are almost fixed, so that the number of antennas needs to be increased according to requirements, which ultimately makes it difficult to achieve electromagnetic compatibility between subsystems and affect antenna performance. Reconfigurable antennas provide a good solution for eliminating the limitations of a single type of antenna, improving system performance, reducing system weight and footprint. Thus, polarized reconfigurable antennas, frequency reconfigurable antennas, directional reconfigurable antennas, and hybrid reconfigurable antennas were born [15]–[18]. Recently, the concept of OAM mode reconfigurable antennas was first proposed to generate two modes simultaneously at 2.4GHz [19]. Subsequently, a mechanically reconfigurable array antenna was proposed to generate multi-mode OAM [20].

The objective of the present work paper is to design an electronically mode reconfigurable antenna, which can generate five OAM modes, namely $l = 0, \pm1$, and ±2. The mode reconfigurable function is realized by controlling the coding sequence of the corresponding PIN diode DC bias voltage on the RFN. There are ninety-six (forty-eight pairs) PIN diodes on the RFN to dynamically change the OAM transmitting modes, all PIN diodes are controlled by a direct current (DC) control board. In practice, a programmable microcontroller hardware (STM32F103V8) was used to provide $+1.4$V or -1.4V DC voltage to every pair PIN diode individually, hence, the OAM transmitting mode can be controlled by the microcontroller.

II. ANTENNA STRUCTURE AND DESIGN CONSIDERATIONS

The overall structure of the proposed reconfigurable OAM array antenna is set out in Fig.1. The antenna structure is supported by three-layer stacked dielectric substrates, which is substrate 1, substrate 2, and substrate 3 from bottom to top. The electrical structure part is RFN (Plane-A), ground plane (Plane-B), rectangular coupling patch (plan-C), and circular radiation patch (Plane-D) from bottom to top. Dielectric substrate parameters, such as substrate thickness, relative dielectric constant, and loss tangent are indicated by H_i, ε_i, $\tan\delta_i$, respectively, where i takes 1, 2, and 3. The thinner dielectric substrate of the lowermost supported RFN is designed to prevent surface wave mode propagation from reducing antenna gain and affecting impedance matching. An exploded view of the array antenna displayed in Fig.2 is provided to further illustrate the design principle of the proposed antenna.

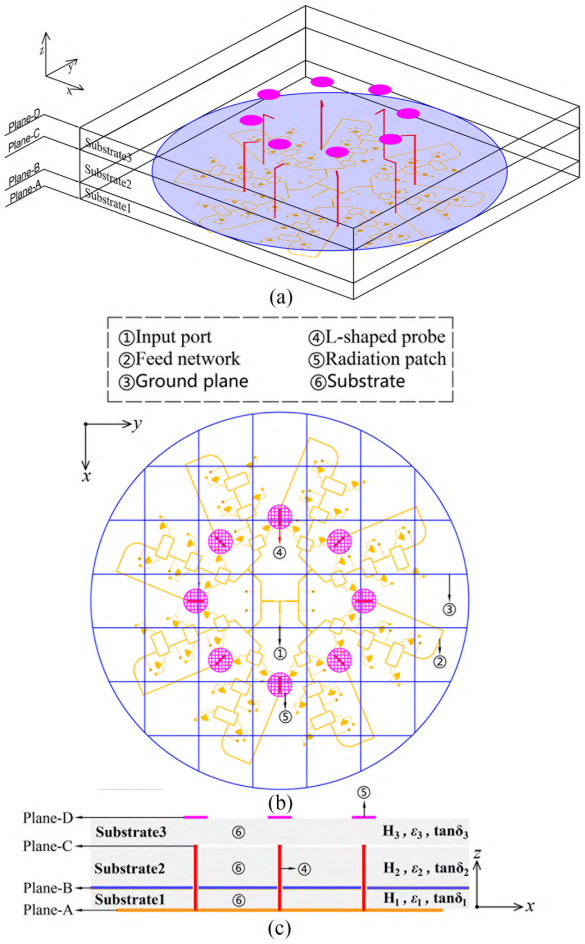

FIGURE 1. Configuration of reconfigurable OAM antenna. (a) Perspective view, (b) Top view, (c) Side view.

A. CONFIGURATION OF THE RFN

It can be seen from Figs.2(a) that the array parallel feed network consists of a three-stage T-Junction power divider and twenty-four switched line phase shifters. A simple equivalent transmission line model of the RFN is set out in Figure 3. For the bias circuit and DC loop, please refer to Figure 2(a), which is not given in Figure 3. As can be seen from Figs.2(a) and 3, the first three-stage power divider with eight output ports $P_{A,B,C,D,E,F,G,H}$ constitutes the main feed network counting from input port P_{in}. Then, each output is connected in series with a reconfigurable sub-network (RSN), which consists of three switched line phase shifters. Finally, the signal flows through the eight RSNs to the corresponding eight output ports P_1 to P_8. The angle between adjacent output ports and RSNs is 45° with radial symmetry. Since all eight RSNs have the same topology, for the sake of simplicity, only the RSN_1 corresponding to the array element 1 is shown in Fig.3.

The RSN comprises a 45°, a 90°, and a 180° switched line phase shifter with reconfigurable function. Four (two pairs) PIN diodes connect the reference line and delay-line of each switched line phase shifter to the middle microstrip line. The arrangement of all PIN diodes on the RSN is same as

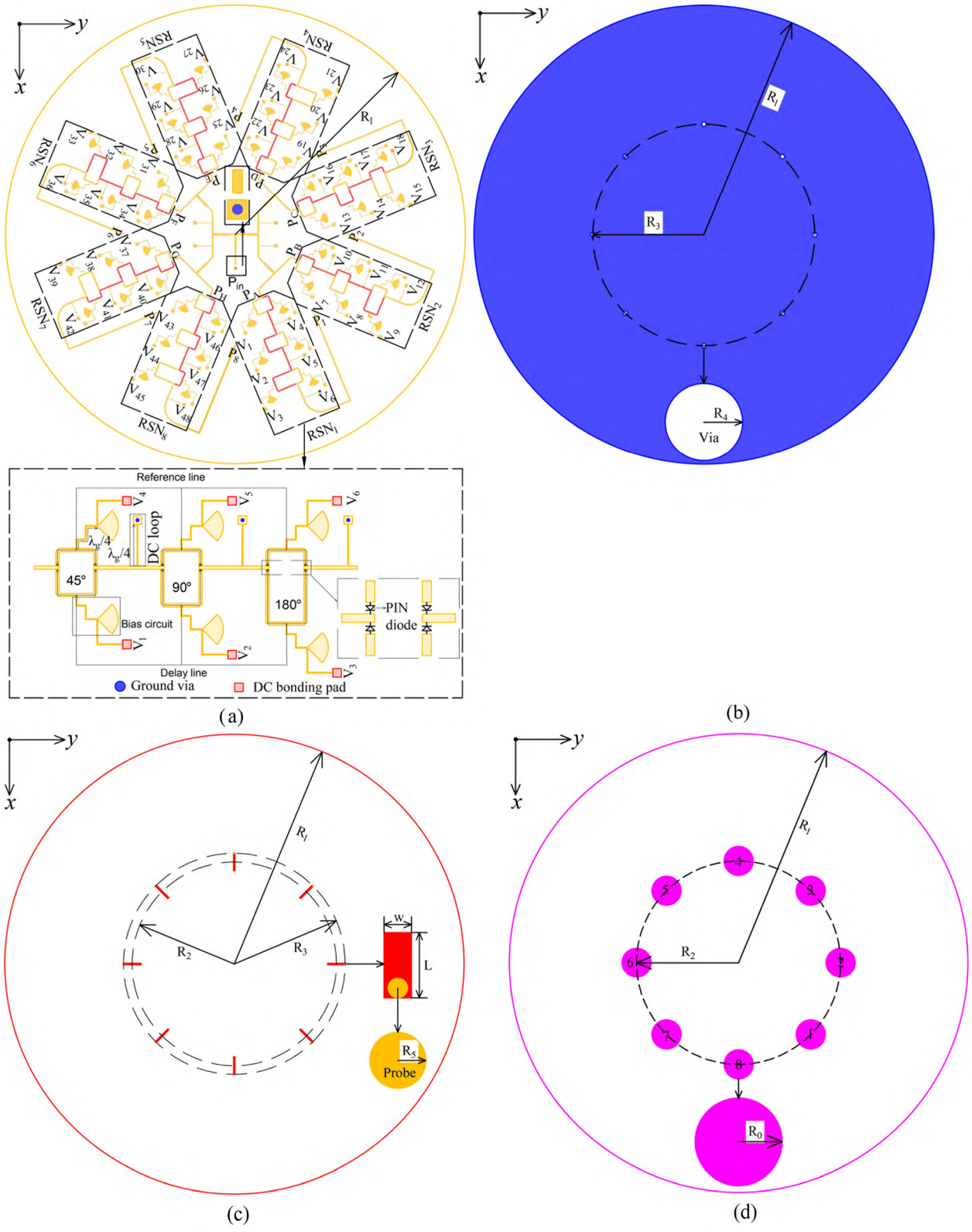

FIGURE 2. Structures of the substrates. (a) Plane-A, (b) Plane-B, (c) Plane-C, (d) Plane-D.

shown in Fig.2 (a). Therefore, by controlling the on/off state of the PIN diode, the path of the AC signal can be changed such that the phases of the respective output ports are the same or different depending on the OAM mode. Furthermore, the on-off state of the PIN diode is controlled by changing the bias voltage of the DC bias circuit, which consists of

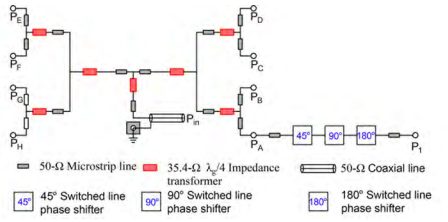

FIGURE 3. Equivalent transmission line topology of the RFN.

a $\lambda_g/4$ sector open-circuited stub and $\lambda_g/4$ high-impedance (100-Ω) line (λ_g is the guided-wavelength at 5.8GHz). There also have $\lambda_g/4$ shorted microstrip line to provide DC loop. The bias circuit and DC loop design method mentioned above is to ensure that the AC signal and the DC signal do not interfere with each other.

B. STRUCTURE OF RADIATION AND COUPLING PATCH

Looking at Figs.1, 2 (c), and 2(d), the rectangular coupling patches with length × width = L × W and the circular radiation patches with radius R1 are located on the upper surfaces of the substrate 2 and the substrate 3, respectively. The distance from the origin to centers of all radial radiating patches and rectangular coupling patches are indicated by R_2. All radiating patches and coupling patches are radially evenly distributed around the z-axis with an angle of 45° between adjacent elements. The output port of the RFN and the coupling patches are electrically connected by vertical copper probes that pass through slots on the ground plane. The L-shaped probe consisting of copper probe and coupling patch is used to stimulate antenna. It is worth noting that the radius R_4 of the slots on the ground plane is larger than the radius R_5 of the copper probes to prevent shorting of the probes.

C. OPERATION PRINCIPLE OF ARRAY ANTENNA

As shown in Figs.1, 2(a), and 3, configuration of the RFN shows that the signal enters from the input port Pin, and is divided into eight signals with the same amplitude and phase when it reaches the input ports $P_{A,B,C,D,E,F,G,H}$ of the eight RSNS after flowing through the main feed network. Finally, each signal flows through the eight RSNS to the output port P_1 to P_8 with equal-amplitude and equal or unequal phase depending on the OAM modes. The phase difference between two adjacent ports can be dynamically reconfigured by changing the bias voltage V_1 to V_{48} of the PIN diodes on the RFN. It is worth noting that each bias voltage control two (a pair) PIN diodes. We take array element 1 as a reference and assume that its initial phase is 0. If the phase of array elements 2 to 8 increases or decreases $\Delta\varphi = 2\pi l/\mathrm{N}$ successively in the anticlockwise direction, where N is the number of array elements in this paper N=8, we can get different positive or negative OAM modes depending on the phase difference $\Delta\varphi$. In order to clarify the reconfigurable characteristics of the proposed OAM antenna, the mode l =2 is taken as an example for illustration, if the bias voltages are set as

$$V_{1,5,6,7,8,12,13,15,17,19,20,21,25,29,30,31,32,36,37,39,41,43,44,45} = -1.4\mathrm{V},$$

$$V_{2,3,4,9,10,11,14,16,18,22,23,24,26,27,28,33,34,35,38,40,42,46,47,48} = 1.4\mathrm{V},$$

each signal will flows through the red path of eight RSNS as set out in Fig.2 (a), and the phase between adjacent array elements is linearly advanced 90° anticlockwise. Table 1 shows the feed phase difference of two adjacent array elements corresponding to all OAM modes that can be generated by the proposed OAM antenna. In practice, a programmable microcontroller hardware (STM32F103V8) was used to provide +1.4V or -1.4V DC voltage to every pair PIN diode individually to achieve reconfigurable functions in different OAM modes. We can use the binary numbers '1' and '0' to represent 1.4V and −1.4V, respectively [21]. The coding sequences of all OAM modes generated by the proposed array antenna are summarized in Table 2.

TABLE 1. Phase difference between adjacent array elements corresponding to different OAM modes.

OAM mode	Phase delay ($\Delta\varphi=2\pi l/\mathrm{N}$)	Phase shift between nearby elements
l=-2	-90°	φ_N-φ_{N-1}=-90°
l=-1	-45°	φ_N-φ_{N-1}=-45°
l=0	0°	φ_N-φ_{N-1}=0°
l=1	45°	φ_N-φ_{N-1}=45°
l=2	90°	φ_N-φ_{N-1}=90°

III. FULLWAVE SIMULATION AND MEASUREMENT

The theoretical proof that a radially uniform circular array can produce OAM vortex beams is given in [9]. The full-wave solver HFSS based on the finite element method is used to numerically simulate the OAM antenna shown in Figure 1, and the values of the antenna structure parameters are list in Table 3. The substrate1 is Rogers 5880, with relative permittivity $\varepsilon_1 = 2.2$, loss tangent $\tan\delta_1 = 0.0009$, and thickness $H_1 = 0.254$mm. The substrate2 and substrate3 are F4T-220, with relative permittivity $\varepsilon_2 = \varepsilon_3 = 2.2$, loss tangent $\tan\delta_2 = \tan\delta_3 = 0.0009$, and thickness $H_2 = 2$mm, thickness $H_3 = 0.5$mm. All three layer substrates are round with a radius of $R_1 = 145$mm. The PIN diodes MA4PBL027 with Beam Lead Die package from MACOM are used as the reconfigurable switch. According to the manufacturer, the diode's equivalent circuit is modeled by a series resistance ($R_S = 3\Omega$) with a series inductance ($L_S = 1.1$nH) in On-state, and a series capacitance ($C_S = 0.03$pF) with a series inductance ($L_S = 1.1$nH) in Off-state. In the simulation, the equivalent circuit when the PIN diode is in the on or off state is simulated by assigning the lumped RLC boundary condition.

Fig.4 shows the simulation results of the transmission coefficient of the reconfigurable feed network for

TABLE 2. Coding sequences of all OAM modes.

OAM modes \ Coding sequences	V_1-V_6	V_7-V_{12}	V_{13}-V_{18}	V_{19}-V_{24}	V_{25}-V_{30}	V_{31}-V_{36}	V_{37}-V_{42}	V_{43}-V_{48}
l=-2	000111	010101	001110	011100	000111	010101	001110	011100
l=-1	000111	100011	010101	110001	001110	101010	011100	111000
l=0	000111	000111	000111	000111	000111	000111	000111	000111
l=1	111000	011100	101010	001110	110001	010101	100011	000111
l=2	011100	001110	010101	000111	011100	001110	010101	000111

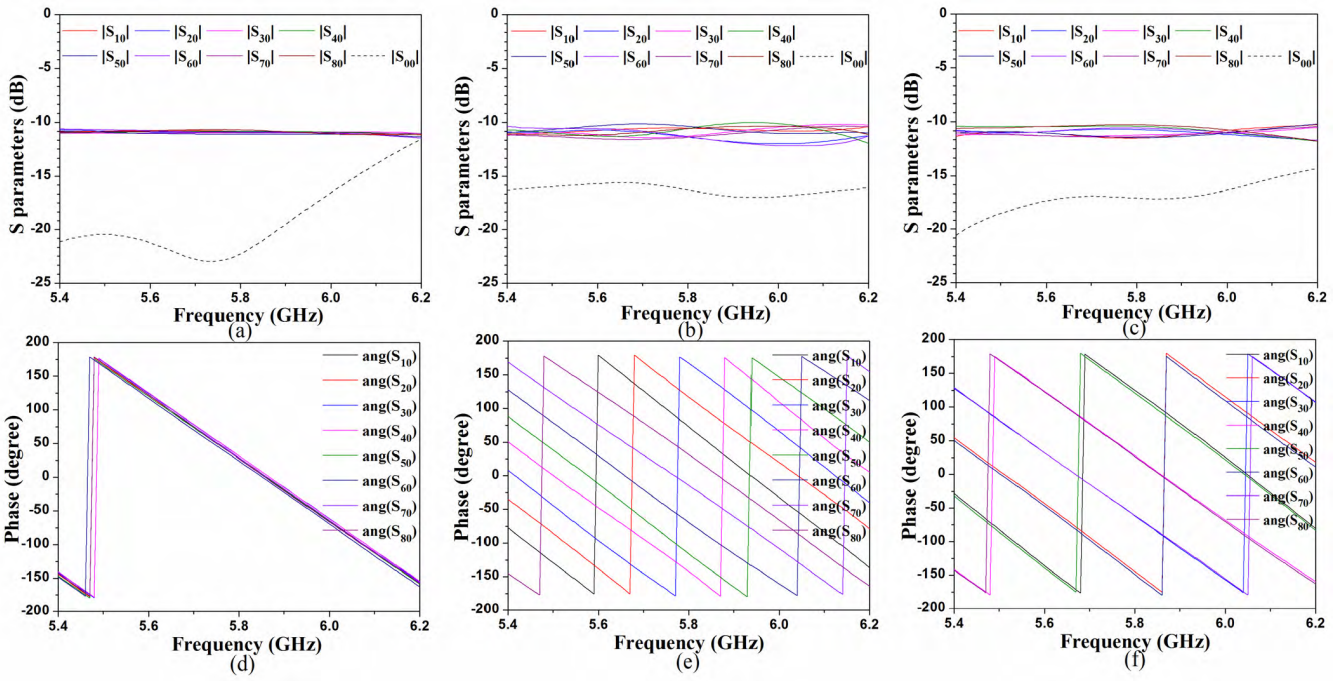

FIGURE 4. Simulation results of the reconfigurable feed network. (a) S parameters of $l = 0$, (b) S parameters of $l = 1$, (c) S parameters of $l = 2$, (d) Phases of $l = 0$, (e) Phases of $l = 1$, (f) Phases of $l = 2$.

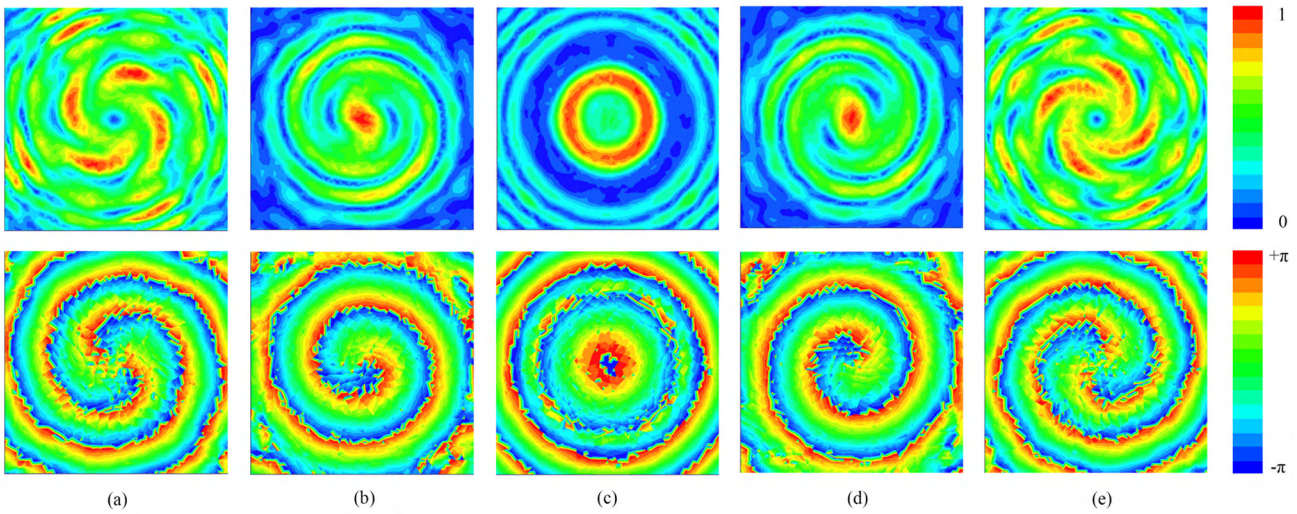

FIGURE 5. Simulated electric field normalized magnitude (upper) and phase (lower) distribution at 5.8 GHz for (a) $l = -2$, (b) $l = -1$, (c) $l = 0$, (d) $l = 1$, (e) $l = 2$.

modes $l = 0$, 1, and 2. The input port P_{in} in Fig. 2 (a) is here denoted by P_0. It can be seen that the magnitude imbalance of the transmission coefficient for all OAM modes is very small in the frequency band form 5.4 GHz to 6.2 GHz, indicating that each array element is equal magnitude feed. The phase deviation of the designed reconfigurable feed network for all

TABLE 3. Design parameter values of the OAM antenna (Size: mm).

R_0	R_1	R_2	R_3	R_4	R_5	L	W
9.15	145	64.55	70	1.5	0.5	12	1.515

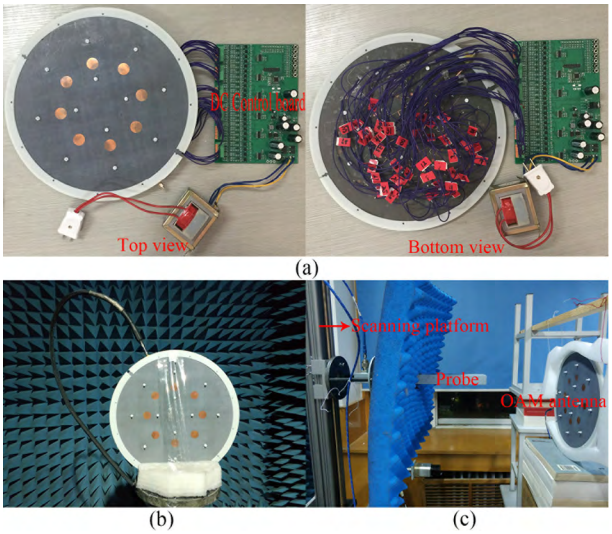

FIGURE 6. (a) Top and bottom views of the fabricated antenna, (b) Measurement setup in far-field, (c) Measurement setup in near-field.

OAM modes is ±4° in the frequency band form 5.4 GHz to 6.2 GHz. Since modes $l = -1$ and $l = -2$ have the same characteristics as modes $l = 1$ and $l = 2$ except for opposite phase shifts, so not given in Fig.4.

Fig.5 shows the simulation results of the normalized amplitude and phase distribution of the electric field generated by the proposed reconfigurable OAM antenna at 5.8GHz. The observed plane is a square of 500 mm × 500 mm with a distance of 300 mm directly above the upper surface of the antenna. From the phase distribution of the electric field in the second row of Fig. 5, the spiral phase wavefront can be clearly seen, and according to the periodic phase change number and the change direction along the azimuth direction, it can be seen that the proposed OAM antenna can generate the vortex electromagnetic beams with $l = 0, \pm 1$, and ± 2 modes. An interesting phenomenon can be seen from the amplitude distribution of the electric field, that is, when the mode $l = \pm 1$, there is no amplitude null, and when the mode $l = 0$, the amplitude null occurs. The reason for this phenomenon has been explained in [9].

The prototype of the proposed reconfigurable OAM antenna was fabricated using PCB processing as set out in Fig.6 (a). Assemble each layer substrate with plastic screws. The reflection coefficient $|S_{11}|$ was measured by a vector network analyzer of Agilent E5071C. The far-field radiation pattern is measured in the anechoic chamber, and the measurement setup is shown in Fig.6 (b). The +1.4V or −1.4V bias voltage of the PIN diode is provided by the DC control board and programmed according to the code sequence of Table 2. The output current of all output ports of the DC control board is 32mA.

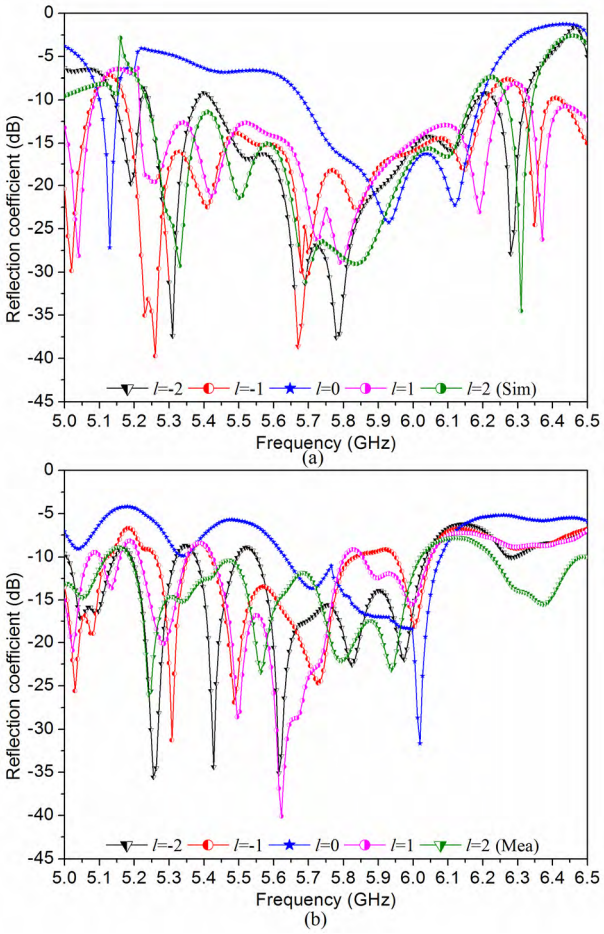

FIGURE 7. Simulated and measured reflection coefficient in different OAM modes. (a) Simulation result, (b) Measurement result.

The simulated and measured reflection coefficients of the reconfigurable OAM antenna at different modes are set out in Fig.7. For the modes $l = \pm 1$ and $l = \pm 2$, the measured reflection coefficient $|S_{11}| < -10$ dB has a frequency range of 5.25 GHz to 6.1 GHz, and for the mode $l = 0$, the frequency range is 5.65 GHz to 6.1 GHz. The simulation and measurement results of the reflection coefficient |S11| <−10 dB are almost the same at low frequencies for all modes, except that the simulation results are larger than the measurement results by about 100 MHz at high frequencies. It can be seen that the designed antenna has a relatively large working bandwidth.

The simulated and measured far-field radiation patterns of the proposed antenna at the frequency 5.8GHz for the modes $l = -2$, $l = -1$, and $l = 0$ are set out in Fig.8. It can be seen that the simulation results are basically consistent with the measurement results. The far-field patterns of modes $l = 1$ and $l = 2$ are basically the same as the far-field patterns of modes $l = 1$ and $l = 2$, so measurement is not performed. The maximum gains of the OAM mode for $l = -2, -1$, and 0 are 6.2dBi, 11.3dBi, and 9.6dBi, respectively. It is can be seen from Fig.8 that the main lobe of modes $l = -1$ and $l = 0$ are point to the direction of $\theta = 0°$ and $\theta = \pm 13°$,

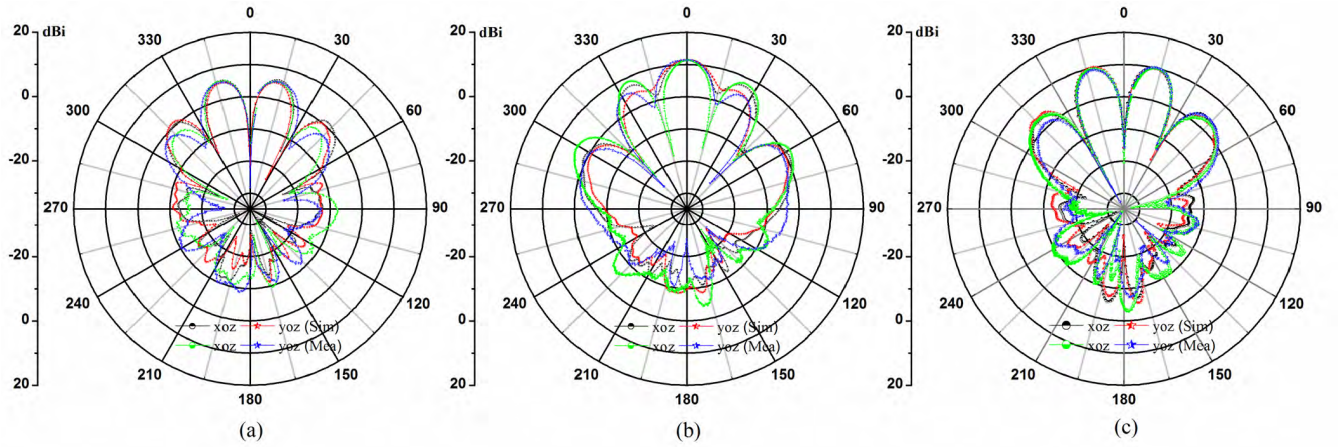

FIGURE 8. Far-field radiation pattern in different modes at 5.8 GHz. (a) $l = -2$, (b) $l = -1$, (c) $l = 0$.

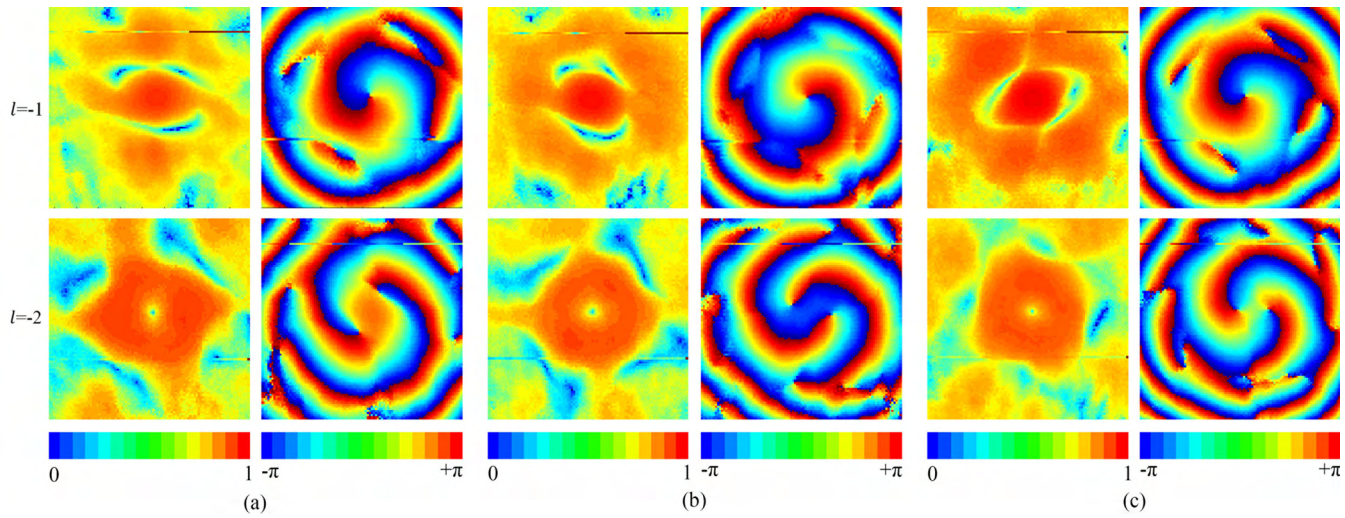

FIGURE 9. Measured electric field normalized magnitude and phase distribution at different frequencies. (a) 5.5 GHz, (b) 5.8 GHz, (c) 6.1 GHz.

respectively, while the radiation patterns of the reported OAM antennas possess a null at $\theta = 0°$ for mode $l = -1$ and main lobe for mode $l = 0$ point to the direction of $\theta = 0°$. This phenomenon is similar to the amplitude distribution of the electric field mentioned above and the reason also has been illustrated in [9].

In this paper, the planar near-field scanning experiment is carried out when the antenna works in the modes $l = -2$ and $l = -1$. The experimental test diagram is shown in Figure 6(c). The array antenna is fixed on the dielectric support. In the experiment, the open waveguide is used as the standard near-field measurement probe. The center axis of the OAM antenna is aligned with the center axis of the waveguide and is 300mm apart. Probe sampling size is 500mm × 500mm, sampling interval is 5mm. To illustrate that the proposed antenna is capable of generating OAM over a wide frequency band, the amplitude and phase distribution of the electric field at three frequencies is measured in the experiment, as shown in Fig.9. Due to the limitation of the phase shift bandwidth of the RFN, the OAM generated bandwidth is smaller than the −10dB reflection coefficient bandwidth. There are some problems compared with the simulation results. It can be seen that the spiral on the observation surface is not smooth and flat. The main reason for this problem is that the sampling interval is too large. If the near field measurement uses smaller sampling interval, the effect of the phase distribution map of the electric field will be closer to the simulation result.

IV. CONCLUSION

This paper proposes an antenna that can generate multiple OAM modes and has electrically controlled mode reconfigurable function by designing a RFN using multiple PIN diodes as a reconfigurable switch. With altering the coding sequence of the corresponding PIN diode DC bias voltage on the RFN using a programmable microcontroller, the proposed antenna has generated five modes in a wide frequency band. Different from the previous method of generating multiple

OAM modes using multiple circular arrays with respective feed networks or one circular array requiring multiple phase shifters, this paper implements a scheme for generating multiple OAM modes with a single antenna through the design of a RFN. The measurement results prove that the proposed design method is feasible.

REFERENCES

[1] A. M. Yao and M. J. Padgett, "Orbital angular momentum: Origins, behavior and applications," *Adv. Opt. Photon.*, vol. 3, no. 3, pp. 161–204, Jun. 2011.
[2] L. Allen, M. W. Beijersbergen, R. Spreeuw, and J. Woerdman, "Orbital angular momentum of light and the transformation of Laguerre-Gaussian laser modes," *Phys. Rev. A, Gen. Phys.*, vol. 45, no. 11, pp. 8185–8189, Jun. 1992.
[3] B. Thidé *et al.*, "Utilization of photon orbital angular momentum in the low-frequency radio domain," *Phys. Rev. Lett.*, vol. 99, no. 8, p. 087701, Aug. 2007.
[4] X. Hui *et al.*, "Ultralow reflectivity spiral phase plate for generation of millimeter-wave OAM beam," *IEEE Antennas Wireless Propag. Lett.*, vol. 14, pp. 966–969, 2015.
[5] Y. Chen *et al.*, "A flat-lensed spiral phase plate based on phase-shifting surface for generation of millimeter-wave OAM beam," *IEEE Antennas Wireless Propag. Lett.*, vol. 15, pp. 1156–1158, 2016.
[6] F. Tamburini, E. Mari, B. Thidé, C. Barbieri, and F. Romanato, "Experimental verification of photon angular momentum and vorticity with radio techniques," *Appl. Phys. Lett.*, vol. 99, no. 20, p. 204102, 2011.
[7] Q. Bai, A. Tennant, and B. Allen, "Experimental circular phased array for generating OAM radio beams," *Electron. Lett.*, vol. 50, no. 20, pp. 1414–1415, 2014.
[8] Y. Gong *et al.*, "Generation and transmission of OAM-carrying vortex beams using circular antenna array," *IEEE Trans. Antennas Propag.*, vol. 65, no. 6, pp. 2940–2949, Jun. 2017.
[9] Z.-G. Guo and G.-M. Yang, "Radial uniform circular antenna array for dual-mode OAM communication," *IEEE Antennas Wireless Propag. Lett.*, vol. 16, pp. 404–407, 2017.
[10] W. Zhang *et al.*, "Four-OAM-mode antenna with traveling-wave ring-slot structure," *IEEE Antennas Wireless Propag. Lett.*, vol. 16, pp. 194–197, May 2016.
[11] J. Ren and K. W. Leung, "Generation of microwave orbital angular momentum states using hemispherical dielectric resonator antenna," *Appl. Phys. Lett.*, vol. 112, no. 13, p. 131103, 2018.
[12] J. Liang and S. Zhang, "Orbital angular momentum (OAM) generation by cylinder dielectric resonator antenna for future wireless communications," *IEEE Access*, vol. 4, pp. 9570–9574, 2016.
[13] Y. Pan *et al.*, "Generation of orbital angular momentum radio waves based on dielectric resonator antenna," *IEEE Antennas Wireless Propag. Lett.*, vol. 16, pp. 385–388, 2017.
[14] Y. Shi and Y. Zhang, "Generation of wideband tunable orbital angular momentum vortex waves using graphene metamaterial reflectarray," *IEEE Access*, vol. 6, pp. 5341–5347, 2018.
[15] C. N. Álvarez, R. Cheung, and J. S. Thompson, "Performance analysis of hybrid metal–graphene frequency reconfigurable antennas in the microwave regime," *IEEE Trans. Antennas Propag.*, vol. 65, no. 4, pp. 1558–1569, Apr. 2017.
[16] C. Wu, Z. Yang, Y. Li, Y. Zhang, and Y. Yashchyshyn, "Methodology to reduce the number of switches in frequency reconfigurable antennas with massive switches," *IEEE Access*, vol. 6, pp. 12187–12196, 2018.
[17] M. A. Hossain, I. Bahceci, and B. A. Cetiner, "Parasitic layer-based radiation pattern reconfigurable antenna for 5G communications," *IEEE Trans. Antennas Propag.*, vol. 65, no. 12, pp. 6444–6452, Dec. 2017.
[18] W. Li *et al.*, "Polarization-reconfigurable circularly polarized planar antenna using switchable polarizer," *IEEE Trans. Antennas Propag.*, vol. 65, no. 9, pp. 4470–4477, Sep. 2017.
[19] B. Liu, G. Lin, Y. Cui, and R. Li, "An orbital angular momentum (OAM) mode reconfigurable antenna for channel capacity improvement and digital data encoding," *Sci. Rep.*, vol. 7, p. 9852, Aug. 2017.
[20] L. Li and X. Zhou, "Mechanically reconfigurable single-arm spiral antenna array for generation of broadband circularly polarized orbital angular momentum vortex waves," *Sci. Rep.*, vol. 8, Mar. 2018, Art. no. 5128.
[21] J. Hu, Z.-C. Hao, and Y. Wang, "A wideband array antenna with 1-bit digital-controllable radiation beams," *IEEE Access*, vol. 6, pp. 10858–10866, 2018.

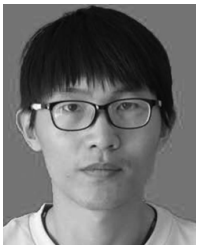

YAN-YANG WANG received the B.S. degree in communication engineering from the Inner Mongolia University of Science and Technology, Baotou, China, in 2016, where he is currently pursuing the M.S. degree in computer science and technology. His current research interests include orbital angular momentum antennas and smart antenna technology.

YONG-XING DU received the B.S. degree in communication engineering from the Chengdu University of Information Technology, Chengdu, China, in 2001, and the M.S. degree in electronic circuit and system and the Ph.D. degree in microelectronics and solid electronics from the Xi'an University of Technology, Xi'an, China, in 2007 and 2014, respectively.

From 2001 to 2007, he was a Research Assistant and from 2007 to 2012, he was a Lecturer with the School of Information Engineering, Inner Mongolia University of Science and Technology, Baotou, respectively, where he has been an Associate Professor since 2012. He has authored one book, over 30 articles, and nine inventions. His current research interest is smart antenna technology.

LING QIN received the B.S. degree in communication engineering from the Chengdu University of Information Technology, Chengdu, China, in 2001, and the M.S. degree in automation from the Xi'an University of Technology, Xi'an, China, in 2007, and the Ph.D. degree in automation from Chang'an University, Xi'an, in 2017.

From 2007 to 2012, she was a Lecturer with the School of Information Engineering, Inner Mongolia University of Science and Technology, Baotou, where she has been an Associate Professor since 2012. She is the author of over six articles. Her research interest is optical communication technique.

BAO-SHAN LI received the B.S. degree in radio technology from the Northeastern University, Shenyang, China, in 1986, and the M.S degree in communication engineering from the Inner Mongolia University of Technology, Hohhot, China, in 2007. His current research interest is the application research of RFID and Internet of Things technology.